The Astrophysical Journal, 718:683–694, 2010 August 1 doi:10.1088/0004-637X/718/2/683

THE EDGE OF THE YOUNG GALACTIC DISK

Giovanni Carraro[1,6], Ruben A. Vázquez[2], Edgardo Costa[3], Gabriel Perren[4,7], and André Moitinho[5]
[1] ESO, Alonso de Cordova 3107, 19100 Santiago de Chile, Chile
[2] Facultad de Ciencias Astronómicas y Geofísicas (UNLP), Instituto de Astrofísica de La Plata (CONICET, UNLP), Paseo del Bosque s/n, La Plata, Argentina
[3] Departamento de Astronomía, Universidad de Chile, Casilla 36-D, Santiago, Chile
[4] Instituto de Física de Rosario, IFIR (CONICET-UNR), Parque Urquiza, 2000 Rosario, Argentina
[5] SIM/IDL, Faculdade de Ciências da Universidade de Lisboa, Ed. C8, Campo Grande, 1749-016 Lisboa, Portugal
Received 2009 August 17; accepted 2010 June 2; published 2010 July 6

ABSTRACT

In this work, we report and discuss the detection of two distant diffuse stellar groups in the third Galactic quadrant. They are composed of young stars, with spectral types ranging from late O to late B, and lie at galactocentric distances between 15 and 20 kpc. These groups are located in the area of two cataloged open clusters (VdB–Hagen 04 and Ruprecht 30), projected toward the Vela-Puppis constellations, and within the core of the Canis Major overdensity. Their reddening and distances have been estimated by analyzing their color–color and color–magnitude diagrams, derived from deep *UBV* photometry. The existence of young star aggregates at such extreme distances from the Galactic center challenges the commonly accepted scenario in which the Galactic disk has a sharp cutoff at about 14 kpc from the Galactic center and indicates that it extends to much greater distances (as also supported by the recent detection of CO molecular complexes well beyond this distance). While the groups we find in the area of Ruprecht 30 are compatible with the Orion and Norma-Cygnus spiral arms, respectively, the distant group we identify in the region of VdB–Hagen 04 lies in the external regions of the Norma-Cygnus arm, at a galactocentric distance (∼20 kpc) where no young stars have been detected so far in the optical.

Key words: Galaxy: disk – Galaxy: structure – open clusters and associations: general

Online-only material: color figures

1. INTRODUCTION

Although the existence of a conspicuous extinction window in the direction of the third Galactic quadrant (3GQ) has been known for decades (see, e.g., Fitzgerald 1968; Moffat et al. 1979; Janes 1991; Moitinho 2001), it has only recently been fully exploited to probe the structure of the outer Galactic disk in the optical domain. Major results from this observational effort have been the detection of (1) previously unknown spiral features (Carraro et al. 2005; Moitinho et al. 2006; Vázquez et al. 2008) and (2) stellar overdensities: the Canis Major, CMa overdensity (Martin et al. 2004), and the Monoceros Ring (Newberg et al. 2002), both believed to be signatures of past accretion events.

Our research group has contributed substantially to the subject, providing a new picture of the outer disk spiral structure. Briefly, the most important findings are: (1) the outer (Norma-Cygnus) arm has been found to be a grand design spiral feature defined by young stars, (2) the region closer to the Sun, at galactocentric distances smaller than 9 kpc, is dominated by a conspicuous inter-arm structure, the Local (Orion) spiral arm, at $l \sim 245^{\circ}$, and (3) the Perseus arm seems to be defined in the 3GQ by gas and dust and does not appear to be traced by an evident (optical) young stellar population.

Here, we report the detection of two diffuse stellar groups in the 3GQ, containing young stars with spectral types ranging from late O to A0, which lie at galactocentric distances between 15 and 20 kpc, beyond the widely accepted radius of the Galactic disk (14 kpc). The groups are located in the direction of two cataloged open clusters (VdB–Hagen 04 and Ruprecht 30; Dias et al. 2002; see Table 1), projected toward the Vela-Puppis constellations, well within the core of the CMa overdensity.

This is the first time that such a young population is detected in the very outer disk in optical. H I in our Galaxy extends out to galactocentric distances of 25 kpc, and CO clouds have been found out to 20 kpc (Brand & Wouterloot 2007). In the infrared (IR), compact and well-confined regions of star formation have been recently detected by various groups (Snell et al. 2002; Yun et al. 2007, 2009; Brand & Wouterloot 2007), both in the second and in the third Galactic quadrant.

The existence of young star aggregates at such extreme distances from the Galactic center defies the commonly accepted scenario in which the Galactic disk has a sharp cutoff at about 14 kpc from the Galactic center (Robin & Créze 1986a, 1986b; Robin et al. 1992) and indicates that it extends to much greater distances. The meaning of this cutoff has been questioned by Momany et al. (2006), as far as old/intermediate age populations are concerned. We also recall that the absence of structures beyond this distance in model color–magnitude diagrams has been erroneously used as evidence to support the existence of the CMa dwarf Galaxy (Martin et al. 2004). Quite recently, Sale et al. (2010) made use of the IPHAS surveys to address the same point in a statistical way. By using over 40,000 A-type stars they argue that they do not see any abrupt truncation of the stellar density profile.

Along the same vein, but with greater detail provided by the use of multicolor photometry, we study in this work the sparse young population in the (far-) outer disk along two lines of sight and show that the stellar density profile of young stars (earlier than A0) does not drop suddenly at 12–14 kpc from the Galactic center, but smoothly declines out to 20 kpc. Together with the young, sparse population, we confirm the existence and properties of a compact, extremely distant star cluster,

[6] On leave from Dipartimento di Astronomia, Universitá di Padova, Vicolo Osservatorio 5, I-35122 Padova, Italy.
[7] Fellow of the CONICET, Argentina.

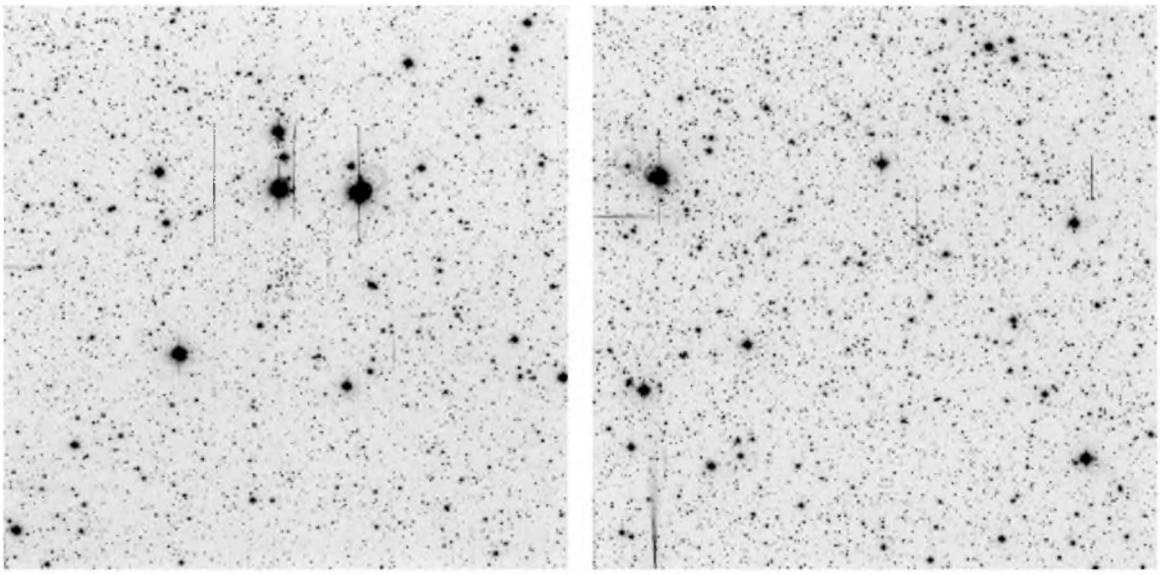

Figure 1. *V* 600 s frame in the region of VdB–Hagen 04 (left) and Ruprecht 30 (right). The FOV is 20′ on a side. North is down and east is to the right.

Table 1
Basic Properties of the Two Fields Studied in This Work

Field	Designation	α(2000.0)	δ(2000.0)	l (deg)	b (deg)	$E(B-V)_{\rm FIRB}$ (mag)	Constellation
Field 1	VdB–Hagen 04	07:37:44	−36:04:00	249.98	−07.13	0.49	Puppis
Field 2	Ruprecht 30	07:42:25	−31:28:00	246.42	−04.05	0.68	Puppis

VdB–Hagen 04, located at more than 20 kpc from the Galactic center.

2. OBSERVATIONS AND DATA REDUCTION

2.1. Observations

The regions of interest (see Figure 1) were observed with the Y4KCAM camera attached to the Cerro Tololo Inter-American Observatory (CTIO) 1.0 m telescope, operated by the SMARTS consortium.[8] This camera is equipped with an STA 4064×4064 CCD with 15 μm pixels, yielding a scale of 0.″289 pixel^{-1} and a field of view (FOV) of 20′ × 20′ at the Cassegrain focus of the CTIO 1.0 m telescope. The CCD was operated without binning, at a nominal gain of 1.44 e^-/ADU, implying a readout noise of 7 e^- per quadrant (this detector is read by means of four different amplifiers). Quantum efficiency and other detector characteristics can be found at http://www.astronomy.ohio-state.edu/Y4KCam/detector.html.

In Table 2, we present the log of the *UBV* observations. All observations were carried out in photometric, good seeing conditions. Typical values for the seeing were 1.1, 1.4, 1.5, and 1.0 for 2008 January 29, January 31, February 1, and February 3, respectively. Our *UBV* instrumental photometric system was defined by the use of a standard broadband Kitt Peak *UBV* set. Transmission curves for these filters can be found at http://www.astronomy.ohio-state.edu/Y4KCam/filters.html. To determine the transformation from our instrumental system to the standard Johnson–Kron–Cousins system, and to correct for extinction, we observed 46 stars in area SA 98 (Landolt 1992) multiple times, and with different airmasses ranging from ∼1.1 to ∼2.6. Field SA 98 is very advantageous, as it includes a large number of well-observed standard stars, and it is completely covered by the CCD's FOV. Furthermore, the standard's color coverage is very good, being $-0.2 \leqslant (B-V) \leqslant 2.2$ and $-0.1 \leqslant (V-I) \leqslant 6.0$.

Table 2
Log of *BVRI* Photometric Observations in the Field of VdB–Hagen 04 and Ruprecht 30

Target	Date	Filter	Exposure (s)	Airmass
VdB–Hagen 04	2008 Jan 29	*U*	10, 20, 100, 200, 900, 1800	1.02–1.04
		B	5, 20, 100, 200, 600, 1800	1.01–1.02
		V	5, 10, 60, 120, 600, 1200	1.01–1.03
SA 98	2008 Jan 29	*U*	2 × 10, 200, 300, 400	1.17–1.96
		B	2 × 10, 100, 2 × 200	1.17–1.89
		V	2 × 10, 100, 2 × 200	1.14–2.12
VdB–Hagen 04	2008 Feb 3	*U*	2 × 10, 60, 200	1.02–1.04
		B	2 × 10, 30, 60	1.01–1.02
		V	2 × 10, 30, 60	1.01–1.03
SA 98	2008 Feb 3	*U*	2 × 10, 200, 300, 400	1.07–1.96
		B	2 × 10, 100, 2 × 200	1.07–1.89
		V	2 × 10, 100, 2 × 200	1.14–2.12
		V	2 × 10, 100, 2 × 200	1.06–2.02
Ruprecht 30	2008 Jan 31	*U*	5, 20, 100, 200	1.10–1.12
		B	5, 10, 60, 120	1.13–1.15
		V	30, 120, 1200	1.13–1.16
SA 98	2008 Jan 31	*U*	2 × 10, 200, 300, 400	1.15–2.20
		B	2 × 10, 100, 2 × 200	1.05–1.79
		V	2 × 10, 100, 2 × 200	1.05–1.79
Ruprecht 30	2008 Feb 1	*U*	30, 600, 1500	1.00–1.00
		B	30, 600, 1500	1.03–1.04
		V	30, 600, 1200	1.01–1.02
SA 98	2008 Feb 1	*U*	2 × 10, 200, 300, 400	1.05–2.11
		B	2 × 10, 100, 2 × 200	1.07–1.69
		V	2 × 10, 100, 2 × 200	1.06–2.02

[6] http://www.astro.yale.edu/smarts

2.2. Reductions

Basic calibration of the CCD frames was done using the Yale/SMARTS y4k reduction script based on the IRAF[9] package CCDRED. For this purpose, zero exposure frames and twilight sky flats were taken every night. Photometry was then performed using the IRAF DAOPHOT and PHOTCAL packages. Instrumental magnitudes were extracted following the point spread function (PSF) method (Stetson 1987). A quadratic, spatially variable, master PSF (PENNY function) was adopted. Aperture corrections were determined making aperture photometry of a suitable number (typically 20–40) of bright, isolated stars in the field. These corrections were found to vary from 0.160 to 0.290 mag, depending on the seeing and filter. The PSF photometry was finally aperture-corrected, filter by filter.

2.3. The Photometry

Both fields were observed on two different nights, all four photometric. We decided to shift observations to a single night for each field, namely, February 3 for VdB–Hagen 04 and January 31 for Ruprecht 30, since these two nights had better seeing.

After removing problematic stars, and stars having only a few observations in Landolt's (1992) catalog, our photometric solution for a grand total of 327 measurements per filter—obtained by combining standard star observations from all nights—turned out to be

$U = u + (3.097 \pm 0.010) + (0.44 \pm 0.01) \times X - (0.040 \pm 0.006) \times (U - B)$,

$B = b + (2.103 \pm 0.012) + (0.27 \pm 0.01) \times X - (0.120 \pm 0.007) \times (B - V)$,

$V = v + (1.760 \pm 0.007) + (0.14 \pm 0.01) \times X + (0.022 \pm 0.007) \times (B - V)$,

for January 31, and

$U = u + (3.090 \pm 0.010) + (0.45 \pm 0.01) \times X - (0.040 \pm 0.006) \times (U - B)$,

$B = b + (2.107 \pm 0.012) + (0.25 \pm 0.01) \times X - (0.111 \pm 0.007) \times (B - V)$,

$V = v + (1.757 \pm 0.007) + (0.15 \pm 0.01) \times X + (0.018 \pm 0.007) \times (B - V)$,

for February 3.

The final rms of the fitting in both cases was 0.050, 0.030, and 0.020 in U, B, and V, respectively.

Global photometric errors were estimated using the scheme developed by Patat & Carraro (2001, Appendix A1), which takes into account the errors resulting from the PSF fitting procedure (i.e., from ALLSTAR), and the calibration errors (corresponding to the zero point, color terms, and extinction errors). In Figure 2, we present global photometric error trends plotted as a function of the V magnitude. Quick inspection shows that stars brighter than $V \approx 20$ mag have errors lower than 0.05 mag in magnitude and lower than 0.10 mag in all colors.

Our final optical photometric catalogs consist of 6039 entries for Ruprecht 30 and 3957 entries for VdB–Hagen 04 having UBV measures down to $V \sim 20$.

Our optical catalog was cross-correlated with the Two Micron All Sky Survey (2MASS; Skrutskie et al. 2006), which resulted in a final catalog including UBV and JHK_s magnitudes. As a by-product, pixel (detector) coordinates were converted to R.A. and decl. for the J2000.0 equinox, thus providing 2MASS-based astrometry.

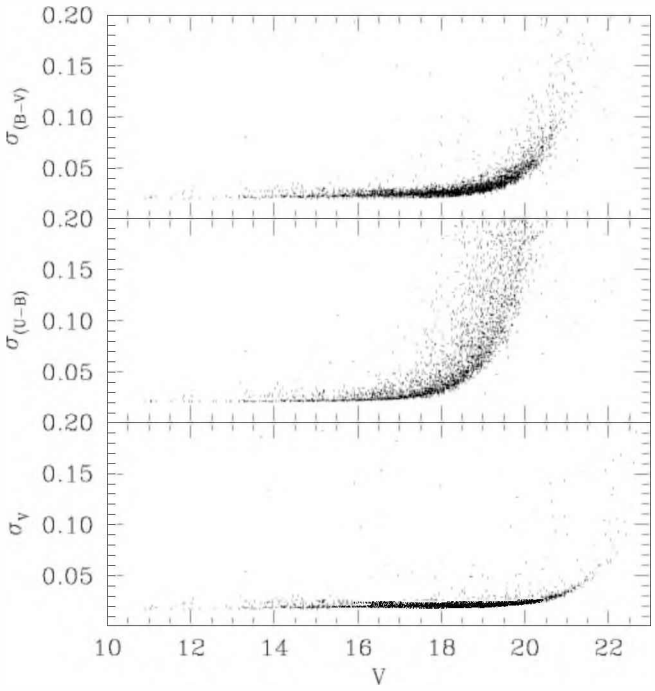

Figure 2. Photometric errors in V, $(B - V)$, and $(U - B)$ as a function of the V magnitude.

Finally, completeness corrections were determined by running artificial star experiments on the data. In brief, we created several artificial images by adding artificial stars to the original frames. These stars were added at random positions, and had the same color and luminosity distribution as the true sample. To avoid generating over-crowding, in each experiment we added up to 20% of the original number of stars. Depending on the frame, between 1000 and 5000 stars were added. In this way, we have estimated that the completeness level of our photometry is better than 50% down to $V = 20.5$.

The two fields in Figure 1 are centered on cataloged Galactic clusters, VdB–Hagen 04 (van den Bergh & Hagen 1975; Carraro & Costa 2007) and Ruprecht 30 (Ruprecht 1966). VdB–Hagen 04 is a compact young cluster whose distance was earlier estimated to be larger than 19.0 kpc from the Sun (Carraro & Costa 2007), based on just V and I photometry. This small color coverage did not allow us to estimate in a solid and precise way the reddening and the distance, since we could only rely on the comparison with isochrones. By performing star counts with the new dataset described in this paper we can confirm that VdB–Hagen is indeed an obvious compact cluster (the left panel of Figure 3), with a radius of about 1.′0 (the right panel of Figure 3). Here, the radius is considered as the distance from the cluster center at which star counts flatten down to the field level. For Ruprecht 30 also, we carried out a similar analysis. Star counts performed in this field do not reveal any obvious overdensity (see Figure 4), demonstrating that there is no cluster at the location of Ruprecht 30.

3. YOUNG GROUPS OF OB STARS IN THE EXTREME PERIPHERY OF THE GALACTIC DISK: THE DETECTION METHOD

The technique that we used to extract information on the stellar populations present in the fields from UBV photometry

[7] IRAF is distributed by the National Optical Astronomy Observatory, which is operated by the Association of Universities for Research in Astronomy, Inc., under cooperative agreement with the National Science Foundation.

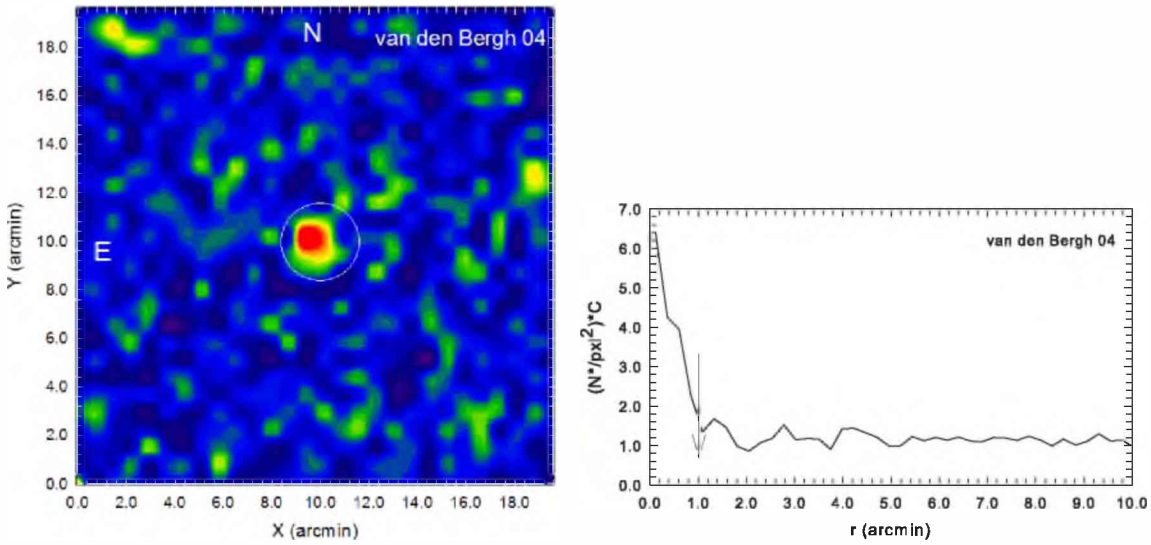

Figure 3. Density map (left) and surface density profile (right) in the area of VdB–Hagen 04.
(A color version of this figure is available in the online journal.)

is old and well established. It combines color–magnitude diagrams (CMDs) and two-color diagrams (TCDs), and its success depends mainly on the availability of U-band photometry. A classical description of this method is given by Straizys (1995), and recent applications of the procedure are illustrated in Vázquez et al. (2005, 2010), Carraro et al. (2007), and Carraro & Costa (2009). Briefly, the starting point is to construct V versus $(B-V)$ CMDs (which as a standalone are difficult to interpret because we are dealing simultaneously with age, distance, reddening, and metallicity effects), and then to construct $(U-B)$ versus $(B-V)$ TCDs in which young blue stars of spectral type earlier than A0 immediately stand out in the upper left part of the diagram. As already demonstrated in previous papers (e.g., the case of the old Galactic cluster Auner 1 in Carraro et al. 2007), a powerful technique is to cut the CMD into 1 mag wide strips and then analyze the TCD for the stars contained in each strip.

The CMDs are shown in Figure 5 for Field 1 (VdB–Hagen 04, left panel) and Field 2 (Ruprecht 30, right panel), where we indicate the location of the Red Giants and Blue Plume stars explicitly to guide the reader. Here, only stars having simultaneous U, B, and V measures with photometric errors smaller than 0.10 mag are shown. The same stars are then plotted in the various panels of Figure 4 for VdB–Hagen 04 and of Figure 5 for Ruprecht 30. In each of the 10 panels in Figures 6 and 7, dashed lines indicate the run of the interstellar reddening for a few spectral-type stars to guide the eye. They are drawn adopting a normal reddening law ($R_V = 3.1$), which has been proven to be valid for the 3GQ ($R_V = 3.1$; Moitinho 2001). The solid line, on the other hand, is an empirical reddening-free, solar metallicity, zero age main sequence from Schmidt-Kaler (1982). We would like to stress however, that in the region of the TCD we are interested in, metallicity effects are negligible, as amply discussed in Carraro et al. (2008).

The advantage of this CMD segmentation is that more distant, hence more reddened, early-type stars immediately stand out and one can easily separate groups of OB stars located at different distances.

To determine reddening, spectral type, and photometric distance we then proceed as follows. First, we derive intrinsic colors

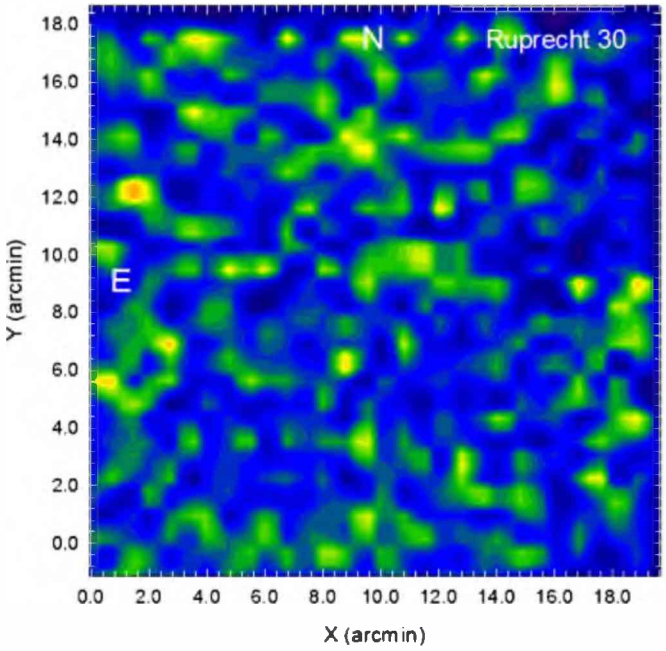

Figure 4. Density map in the area of Ruprecht 30.
(A color version of this figure is available in the online journal.)

using the two relationships:

$$E(U-B) = 0.72 \times E(B-V) + 0.05 \times E(B-V)^2 \quad (1)$$

and

$$(U-B)_0 = 3.69 \times (B-V)_0 + 0.03. \quad (2)$$

The intrinsic color $(B-V)_0$ is the positive root of the second-order equation that one derives by combining the above expressions. Intrinsic colors ($(U-B)_0$ and $(B-V)_0$) are then directly correlated to spectral type, as compiled, for instance, in Schmidt-Kaler (1982). The solution of the above equations, therefore, allows us to encounter stars having spectral types earlier than A0.5. For these stars we then know the absolute magnitude M_V (again from the Schmidt-Kaler 1982 compilation) and, from the

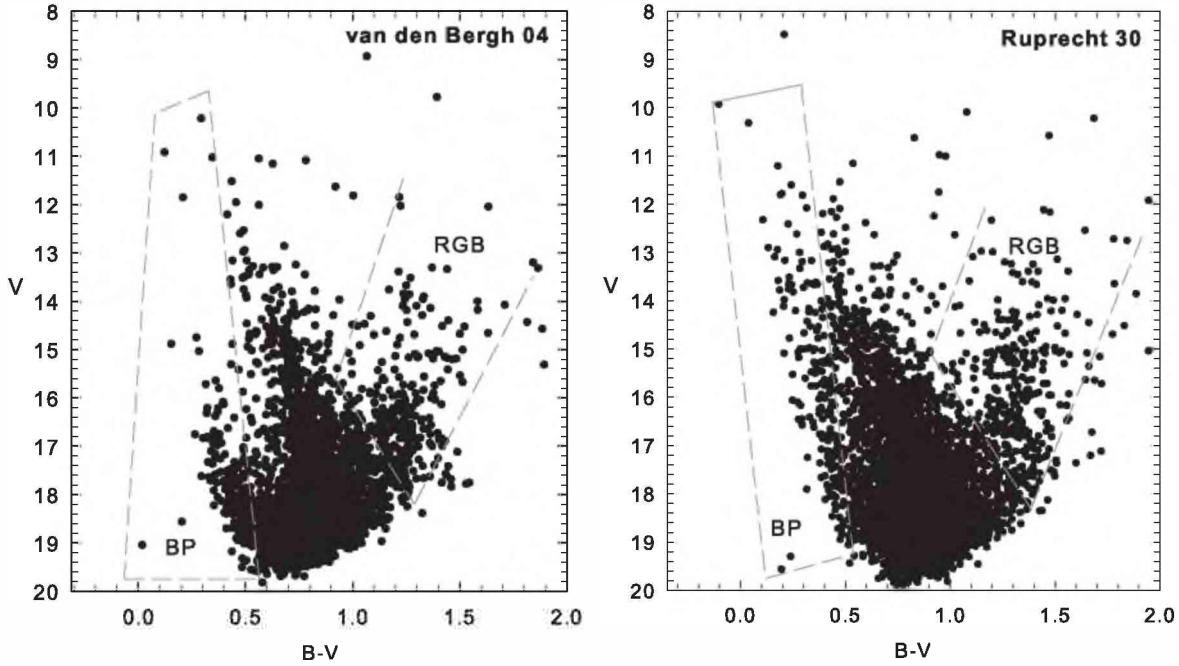

Figure 5. CMDs for Field 1, centered on VdB–Hagen 04 (left panel), and Field 2, centered on Ruprecht 30 (right panel). The regions occupied by the Blue Plume and Red Giant stars are indicated. See the text for more details.

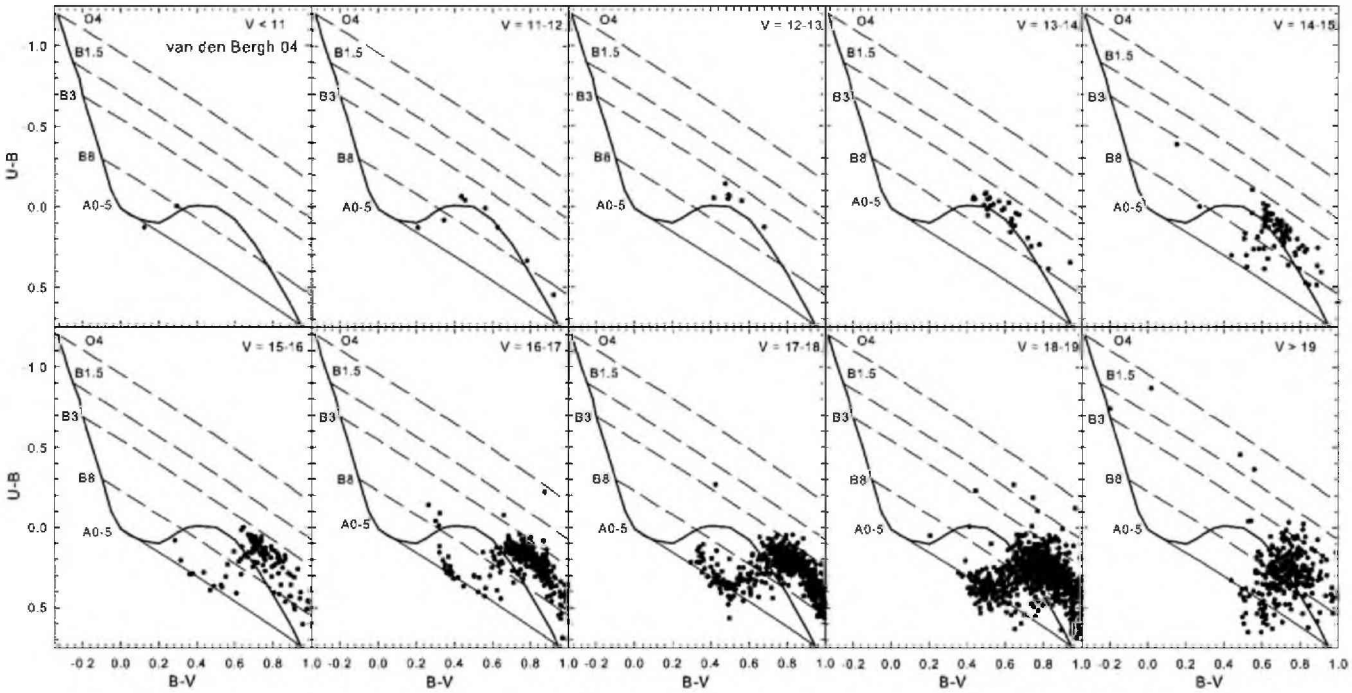

Figure 6. TCDs for all the stars having *UBV* photometry in the field of VdB–Hagen 04 and as a function of the magnitude *V*. Dashed lines show the run of the interstellar reddening for a few typical spectral types, which are indicated.

apparent extinction-corrected magnitude V_0, we finally infer the photometric distance.

Error in distances are computed as follows:

$$\Delta(\mathrm{Dist}) = \ln(10) \times \mathrm{Dist} \times \Delta[\log(\mathrm{Dist})],$$

$$\Delta[\log(\mathrm{Dist})] = \tfrac{1}{5} \times \Delta V + \Delta(M_V) + \Delta(A_V)],$$

$$\Delta(M_V) = 0,$$

$$\Delta(A_V) = 3.1 \times \Delta(B-V), \text{ while}$$

$\Delta(V)$ and $\Delta(B-V)$ directly come from photometry; and finally,

$$\Delta(\mathrm{Dist}) = \ln(10) \times \mathrm{Dist} \times 1/5 \times [\Delta V + 3.1 \times \Delta(B-V)].$$

The results are then summarized in Tables 3 and 4, where we report for any detected early-type star, its ID, magnitude, colors, reddening-corrected colors and magnitude, estimated spectral type and, finally, the heliocentric distance with the associated uncertainty.

In Sections 4 and 5, we will present a qualitative analysis of the results for Field 1 and Field 2, respectively. A quantitative

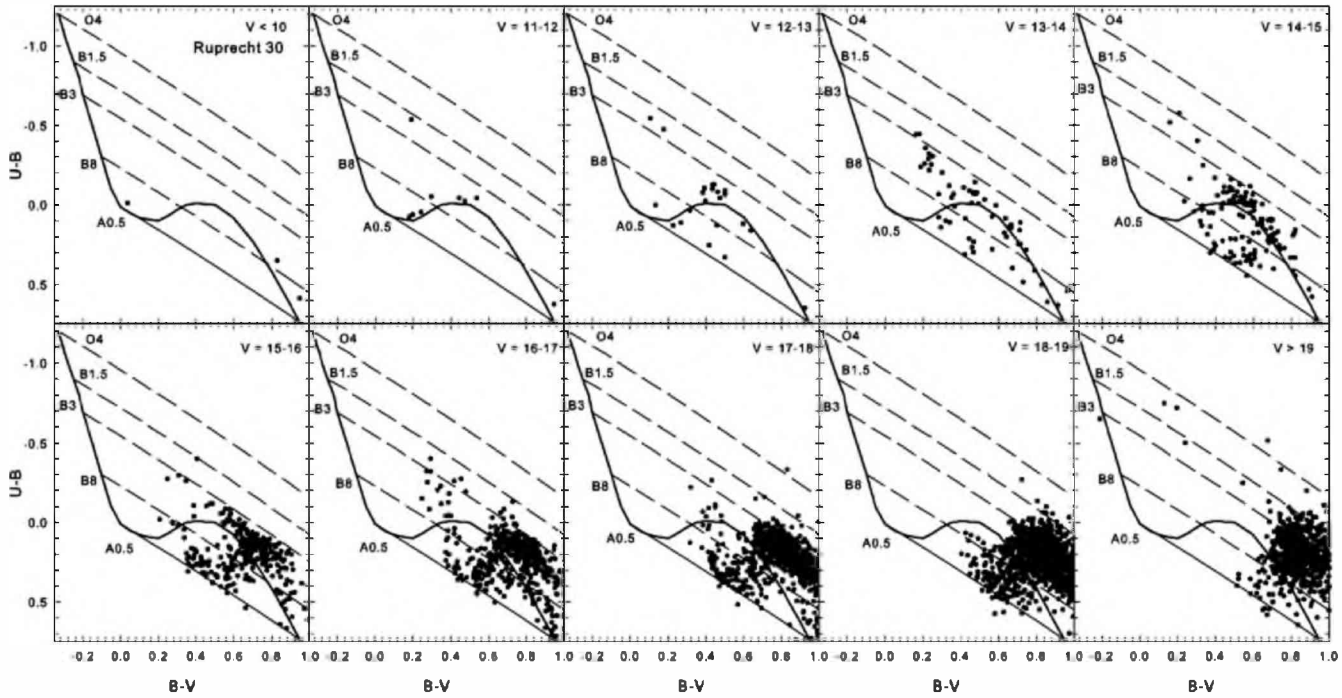

Figure 7. TCDs for all the stars having *UBV* photometry in the field of Ruprecht 30 and as function of the magnitude *V*. Dashed lines show the run of the interstellar reddening for a few typical spectral types, which are indicated.

analysis of the early star distributions in the fields is deferred to Section 6.

4. THE FIELD TOWARD VDB–HAGEN 04

Field 1: This field is centered on the Galactic star cluster VdB–Hagen 04. The overall star distribution seen in the CMD of Field 1 (the left panel of Figure 5) is typical of stellar fields in the 3GQ (Moitinho 2001; Moitinho et al. 2006; Carraro et al. 2007, 2008). Apart from the obvious main sequence (MS) produced by the nearby stars, the basic features of its CMD are as follows: (1) a prominent bright blue sequence, commonly referred to as the Blue Plume, which is the target of this study, (2) a thick blue MS downward of $V \sim 18$, and (3) a population of Red Giants, showing a significant spread in both color and magnitude.

Moving now to Figure 6, where different TCDs are shown as a function of the magnitude *V*, the following remarks can be made.

1. No stars earlier than A0 can be found for *V* brighter than 14.0 mag.
2. The first stars of the early spectral type start to appear only at $V = 15.0$ and become more and more conspicuous down to $V = 18.0$, where they merge with later spectral-type stars (A to F).
3. Downward of $V = 15$, a group of stars of spectral-type F to G starts to become prominent. These have the typical bell shape already found in similar diagrams for the field in the 3GQ (Carraro et al. 2008).

We were able to isolate 80 stars earlier than A0 to which we could assign a spectral type. Individual estimates of intrinsic colors, reddening, spectral type, and distance are listed in Table 3, together with star IDs, magnitudes, and colors.

Further, in Figure 8, top panel, the run of the reddening as a function of distance is shown. Interestingly, the reddening toward VdB–Hagen 04 does not vary much with distance. It gets to its mean value (0.40 ± 0.07 mag) very close to the Sun, and at larger distances, up to almost 20 kpc, keeps basically constant.

Apart from the obvious central concentration produced by the star cluster VdB–Hagen 04 (see again Figure 3), these early-type stars are evenly distributed across the field implying that the field itself has a clear young component at these large distances.

5. THE FIELD TOWARD RUPRECHT 30

Field 2: The corresponding CMD and TCD for Field 2 are shown in the right panel of Figure 5 and in Figure 7. The Blue Plume in the CMD looks quite different from the one in Figure 3, left panel, for VdB–Hagen 04; it shows a larger color spread, spans a larger range in magnitude, and also extends to fainter magnitudes.

The inspection of Figure 7 allows us to suggest the following.

1. No stars earlier than A0 can be found for *V* brighter than 12.0 mag.
2. A first clear group of early spectral type appears at $V = 13.0$, while a second one is visible at $V = 16.0$.
3. In between, and at *V* fainter than 16.0, there are several late B and early A stars almost everywhere, which then disappear completely at *V* larger than 18.0, where they are mixed with late A and F stars.

We counted 200 stars earlier than A0 in this field, for which we could assign a spectral type. Individual estimates of intrinsic colors, reddening, spectral type, and distance are listed in Table 4, together with star IDs, magnitudes, and colors.

The middle panel of Figure 8 shows the run of the reddening as a function of magnitude. As in the case of VdB–Hagen 04, almost all the reddening accumulates close to the Sun, and then it increases very smoothly with distance up to 20 kpc. The mean reddening is 0.466 ± 0.117 and occurs mostly within 5 kpc from the Sun.

In the same Figure 8, we plot in the bottom panel the same run of the reddening as a function of magnitude, but for the direction

Table 3
Basic Properties of the Early Spectral-type Stars Encountered in Field 1 (VdB–Hagen 04)

ID	V	$B-V$	$U-B$	$E(B-V)$	$(B-V)_0$	$(U-B)_0$	M_V	Phot(ST)	Distance (kpc)	ΔDist
1907	10.22	0.29	−0.01	0.37	−0.09	−0.28	0.62	B8	0.49	0.02
108	11.03	0.35	0.08	0.41	−0.07	−0.22	0.80	B8.5	0.62	0.02
1716	12.60	0.48	−0.14	0.64	−0.19	−0.62	−0.76	B3.5	1.87	0.07
2668	14.89	0.44	0.30	0.45	−0.01	−0.02	1.39	A0	2.66	0.10
2028	15.31	0.43	0.28	0.45	−0.02	−0.05	1.31	A0	3.33	0.13
1377	14.75	0.27	0.00	0.34	−0.08	−0.25	0.70	B8.5	3.95	0.15
2116	15.04	0.28	0.08	0.33	−0.06	−0.16	0.96	B9	4.07	0.15
2026	15.80	0.38	0.29	0.38	0.00	0.01	1.51	A0.5	4.22	0.16
2434	15.72	0.32	0.21	0.33	−0.02	−0.03	1.35	A0	4.67	0.18
118	16.21	0.37	0.28	0.37	0.00	0.00	1.49	A0.5	5.16	0.20
1582	16.38	0.36	0.28	0.36	0.01	0.02	1.54	A0.5	5.57	0.22
1932	16.63	0.42	0.31	0.42	0.00	0.00	1.49	A0.5	5.87	0.23
1009	16.21	0.32	0.16	0.35	−0.04	−0.10	1.14	B9.5	6.25	0.24
3611	17.02	0.49	0.36	0.49	0.00	0.00	1.46	A0.5	6.43	0.26
1396	16.81	0.38	0.30	0.37	0.01	0.02	1.54	A0.5	6.64	0.26
907	16.75	0.38	0.26	0.39	−0.01	−0.02	1.41	A0	6.75	0.27
1975	16.69	0.35	0.23	0.37	−0.02	−0.03	1.35	A0	6.92	0.28
1450	16.93	0.39	0.28	0.39	−0.01	−0.01	1.45	A0.5	7.13	0.28
418	16.89	0.38	0.24	0.39	−0.02	−0.04	1.32	A0	7.41	0.29
2222	16.94	0.35	0.26	0.35	0.00	0.00	1.47	A0.5	7.52	0.29
987	16.83	0.34	0.21	0.36	−0.03	−0.05	1.28	A0	7.70	0.30
458	16.32	0.32	−0.01	0.41	−0.10	−0.31	0.53	B8	8.06	0.31
1891	17.44	0.47	0.33	0.47	−0.01	−0.02	1.41	A0	8.20	0.35
2658	17.48	0.45	0.35	0.45	0.01	0.01	1.53	A0.5	8.21	0.33
1043	17.51	0.44	0.34	0.44	0.01	0.01	1.53	A0.5	8.40	0.33
1902	16.98	0.37	0.18	0.40	−0.04	−0.11	1.10	B9.5	8.45	0.33
1090	14.88	0.15	−0.39	0.33	−0.19	−0.62	−0.78	B3.5	8.47	0.31
2866	17.48	0.43	0.31	0.43	−0.01	−0.01	1.45	A0.5	8.64	0.34
3431	16.83	0.32	0.12	0.37	−0.06	−0.15	0.99	B9	8.74	0.34
1457	17.71	0.47	0.36	0.47	0.00	0.01	1.51	A0.5	8.88	0.36
3029	17.17	0.40	0.19	0.44	−0.05	−0.13	1.04	B9.5	8.94	0.35
1845	17.10	0.34	0.18	0.37	−0.04	−0.09	1.17	B9.5	9.09	0.35
2080	17.52	0.41	0.28	0.42	−0.02	−0.04	1.34	A0	9.36	0.37
2283	17.83	0.47	0.36	0.46	0.01	0.01	1.52	A0.5	9.43	0.38
2038	17.58	0.42	0.29	0.43	−0.01	−0.02	1.39	A0	9.45	0.37
2133	17.66	0.42	0.31	0.42	0.00	0.00	1.47	A0.5	9.47	0.37
1612	17.75	0.47	0.33	0.47	−0.01	−0.02	1.41	A0	9.47	0.39
1031	17.33	0.33	0.22	0.34	−0.02	−0.03	1.36	A0	9.62	0.37
3885	17.65	0.46	0.28	0.48	−0.03	−0.08	1.21	B9.5	9.80	0.40
2616	17.24	0.36	0.16	0.40	−0.05	−0.13	1.06	B9.5	9.81	0.38
1970	17.74	0.44	0.30	0.45	−0.02	−0.03	1.37	A0	9.96	0.41
3586	17.16	0.36	0.11	0.42	−0.07	−0.20	0.85	B9	10.10	0.39
2725	17.86	0.44	0.31	0.45	−0.01	−0.02	1.40	A0	10.30	0.42
865	17.36	0.35	0.17	0.38	−0.05	−0.11	1.09	B9.5	10.40	0.41
2092	17.99	0.44	0.34	0.44	0.01	0.01	1.53	A0.5	10.50	0.42
1864	18.02	0.48	0.34	0.48	−0.01	−0.01	1.42	A0.5	10.50	0.43
3572	18.01	0.48	0.33	0.49	−0.02	−0.03	1.36	A0	10.60	0.44
2035	16.83	0.30	−0.04	0.40	−0.10	−0.33	0.46	B7.5	10.70	0.80
766	17.71	0.40	0.25	0.42	−0.03	−0.06	1.26	A0	10.70	0.42
1346	17.58	0.36	0.21	0.39	−0.03	−0.07	1.22	A0	10.80	0.43
1806	17.76	0.37	0.26	0.38	−0.01	−0.02	1.41	A0	10.90	0.43
2519	17.64	0.34	0.22	0.36	−0.02	−0.04	1.33	A0	11.00	0.45
2139	18.05	0.42	0.33	0.42	0.01	0.02	1.54	A0.5	11.00	0.44
2498	17.60	0.36	0.19	0.39	−0.04	−0.09	1.17	B9.5	11.10	0.43
2321	17.78	0.43	0.23	0.46	−0.04	−0.11	1.11	B9.5	11.10	0.45
1817	16.80	0.32	−0.09	0.44	−0.13	−0.41	0.15	B6.5	11.40	0.44
1162	18.20	0.45	0.32	0.46	−0.01	−0.02	1.40	A0	11.90	0.49
29	16.76	0.26	−0.14	0.38	−0.13	−0.42	0.11	B6	12.30	0.48
1576	17.65	0.33	0.14	0.37	−0.05	−0.12	1.07	B9.5	12.30	0.48
2027	18.35	0.44	0.34	0.44	0.01	0.02	1.54	A0.5	12.30	0.56
571	18.33	0.45	0.32	0.45	−0.01	−0.01	1.42	A0.5	12.50	0.53
1823	17.72	0.34	0.12	0.38	−0.06	−0.16	0.97	B9	12.90	0.51
3814	18.33	0.44	0.30	0.45	−0.02	−0.03	1.38	A0	13.00	0.55
1446	17.93	0.43	0.15	0.49	−0.07	−0.21	0.81	B8.5	13.20	0.53
1565	18.30	0.41	0.29	0.42	−0.01	−0.02	1.39	A0	13.20	0.54
1892	18.39	0.41	0.31	0.41	0.00	0.00	1.49	A0.5	13.40	0.55
2954	18.14	0.39	0.21	0.42	−0.04	−0.10	1.13	B9.5	13.80	0.63
2165	18.39	0.45	0.28	0.47	−0.03	−0.07	1.23	A0	13.80	0.58
925	18.68	0.46	0.29	0.48	−0.03	−0.07	1.24	A0	15.50	0.68
3673	18.90	0.46	0.34	0.46	−0.01	0.00	1.46	A0.5	16.00	0.74
937	19.18	0.44	0.33	0.44	0.00	0.00	1.49	A0.5	18.50	0.85

Note. The last column indicates the error in distance.

Table 4
Basic Properties of the Early Spectral-type Stars Encountered in Field 2 (Ruprecht 30)

ID	V	$B-V$	$U-B$	$E(B-V)$	$(B-V)_0$	$(U-B)_0$	M_V	Phot(ST)	Distance (kpc)	Δ Dist
781	8.49	0.21	−0.02	0.27	−0.07	−0.21	0.81	B8.5	0.23	0.01
4525	10.32	0.04	−0.01	0.06	−0.03	−0.05	1.28	A0	0.59	0.02
5383	9.93	−0.10	−0.19	−0.05	−0.06	−0.15	0.99	B9	0.66	0.03
1358	11.21	0.18	0.08	0.20	−0.03	−0.07	1.23	A0	0.74	0.03
4683	11.61	0.24	0.05	0.29	−0.06	−0.17	0.94	B9	0.90	0.03
4674	11.79	0.20	0.06	0.23	−0.04	−0.11	1.11	B9.5	0.98	0.04
1945	12.28	0.46	0.13	0.53	−0.08	−0.26	0.67	B8.5	0.99	0.04
1685	12.08	0.32	0.04	0.39	−0.08	−0.25	0.71	B8.5	1.08	0.04
4098	11.82	0.30	−0.05	0.39	−0.10	−0.34	0.43	B7.5	1.09	0.04
5619	12.83	0.42	0.25	0.44	−0.03	−0.07	1.24	A0	1.11	0.04
6027	12.41	0.23	0.13	0.25	−0.02	−0.05	1.31	A0	1.17	0.05
1805	13.22	0.42	0.31	0.42	0.00	0.00	1.48	A0.5	1.22	0.05
1356	12.62	0.27	0.11	0.30	−0.04	−0.11	1.11	B9.5	1.30	0.05
431	12.16	0.43	−0.10	0.58	−0.16	−0.53	−0.34	B4.5	1.38	0.06
1006	12.20	0.39	−0.11	0.53	−0.15	−0.49	−0.20	B5	1.42	0.06
5939	13.36	0.44	0.21	0.48	−0.05	−0.14	1.01	B9	1.48	0.06
1950	13.57	0.46	0.27	0.48	−0.04	−0.09	1.17	B9.5	1.52	0.06
5258	12.59	0.38	−0.08	0.51	−0.14	−0.45	−0.01	B5.5	1.60	0.06
376	13.00	0.28	0.08	0.33	−0.06	−0.16	0.95	B9	1.60	0.06
1203	13.19	0.29	0.14	0.32	−0.04	−0.09	1.16	B9.5	1.61	0.06
2301	13.80	0.47	0.30	0.48	−0.03	−0.06	1.27	A0	1.61	0.07
4915	12.89	0.40	−0.02	0.51	−0.12	−0.40	0.20	B6.5	1.67	0.07
657	13.73	0.47	0.23	0.51	−0.05	−0.14	1.01	B9	1.69	0.07
480	12.90	0.13	0.00	0.17	−0.05	−0.12	1.07	B9.5	1.81	0.07
1216	12.62	0.44	−0.13	0.60	−0.17	−0.57	−0.54	B4	1.83	0.07
1814	13.55	0.42	0.09	0.50	−0.09	−0.28	0.60	B8	1.90	0.08
4755	14.17	0.39	0.28	0.39	−0.01	−0.01	1.44	A0.5	2.00	0.08
4197	13.65	0.34	0.11	0.39	−0.06	−0.18	0.91	B9	2.01	0.08
4148	13.63	0.32	0.10	0.37	−0.06	−0.17	0.94	B9	2.04	0.08
3135	12.94	0.44	−0.13	0.59	−0.17	−0.56	−0.50	B4.5	2.09	0.08
2209	13.19	0.45	−0.09	0.59	−0.16	−0.52	−0.32	B4.5	2.17	0.09
3829	13.33	0.28	−0.07	0.38	−0.11	−0.34	0.40	B7.5	2.24	0.09
5782	13.17	0.34	−0.12	0.47	−0.14	−0.46	−0.06	B5.5	2.27	0.09
1450	13.66	0.37	0.01	0.46	−0.10	−0.33	0.46	B7.5	2.27	0.09
3805	14.35	0.39	0.24	0.41	−0.03	−0.06	1.27	A0	2.30	0.09
1202	14.25	0.36	0.19	0.39	−0.04	−0.10	1.15	B9.5	2.41	0.10
3020	14.71	0.48	0.30	0.50	−0.03	−0.07	1.24	A0	2.44	0.10
2185	13.67	0.35	−0.05	0.46	−0.12	−0.38	0.27	B7	2.49	0.10
2617	14.01	0.38	0.05	0.47	−0.09	−0.30	0.56	B8	2.51	0.10
5869	13.62	0.36	−0.07	0.48	−0.13	−0.42	0.12	B6	2.54	0.10
647	14.23	0.33	0.13	0.37	−0.05	−0.13	1.03	B9	2.59	0.10
187	14.73	0.40	0.26	0.41	−0.02	−0.04	1.32	A0	2.67	0.11
5592	14.14	0.43	0.02	0.53	−0.11	−0.37	0.31	B7	2.73	0.11
757	14.73	0.44	0.23	0.47	−0.05	−0.12	1.08	B9.5	2.75	0.11
263	14.80	0.50	0.22	0.56	−0.07	−0.19	0.86	B9	2.77	0.11
2662	14.16	0.33	0.03	0.40	−0.08	−0.26	0.67	B8.5	2.82	0.11
2766	14.83	0.48	0.21	0.53	−0.06	−0.17	0.92	B9	2.85	0.12
5340	14.54	0.37	0.14	0.42	−0.06	−0.17	0.94	B9	2.89	0.11
4645	11.81	0.19	−0.54	0.43	−0.24	−0.85	−1.84	B2	2.92	0.11
3269	14.43	0.32	0.10	0.37	−0.06	−0.16	0.95	B9	2.94	0.12
4489	14.06	0.41	−0.06	0.53	−0.14	−0.45	0.00	B5.5	3.04	0.12
5642	14.32	0.43	0.00	0.54	−0.12	−0.40	0.19	B6.5	3.10	0.12
4495	14.35	0.44	−0.01	0.56	−0.13	−0.42	0.11	B6	3.18	0.13
2678	13.52	0.23	−0.22	0.37	−0.15	−0.48	−0.16	B5	3.20	0.12
2846	14.07	0.44	−0.08	0.58	−0.16	−0.51	−0.25	B5	3.20	0.13
5539	15.01	0.35	0.23	0.37	−0.02	−0.04	1.34	A0	3.21	0.13
1969	15.16	0.45	0.25	0.48	−0.04	−0.10	1.12	B9.5	3.22	0.13
3561	13.96	0.42	−0.11	0.56	−0.16	−0.52	−0.31	B5	3.23	0.13
2035	15.03	0.39	0.21	0.42	−0.04	−0.10	1.13	B9.5	3.31	0.13
5306	14.62	0.36	0.05	0.44	−0.09	−0.27	0.63	B8	3.35	0.13
3979	15.28	0.38	0.28	0.39	−0.01	−0.01	1.44	A0.5	3.36	0.14
4955	15.17	0.43	0.22	0.46	−0.05	−0.12	1.08	B9.5	3.42	0.14
2356	13.73	0.30	−0.20	0.45	−0.16	−0.53	−0.36	B4.5	3.46	0.15
1654	15.15	0.46	0.17	0.52	−0.07	−0.22	0.80	B8.5	3.51	0.14
314	15.31	0.43	0.24	0.46	−0.04	−0.09	1.16	B9.5	3.52	0.14

Table 4
(Continued)

ID	V	$B-V$	$U-B$	$E(B-V)$	$(B-V)_0$	$(U-B)_0$	M_V	Phot(ST)	Distance (kpc)	Δ Dist
3036	15.57	0.44	0.32	0.45	−0.01	−0.01	1.43	A0.5	3.57	0.14
3547	15.35	0.36	0.26	0.36	−0.01	−0.01	1.44	A0.5	3.59	0.14
1736	13.16	0.21	−0.36	0.39	−0.19	−0.64	−0.85	B3.5	3.63	0.14
405	12.33	0.11	−0.55	0.33	−0.22	−0.78	−1.49	B2.5	3.64	0.14
2852	13.67	0.24	−0.25	0.40	−0.16	−0.54	−0.39	B4.5	3.70	0.14
4252	15.67	0.43	0.32	0.43	0.00	0.00	1.46	A0.5	3.74	0.15
786	13.78	0.19	−0.24	0.32	−0.15	−0.47	−0.08	B5.5	3.75	0.15
3917	14.03	0.39	−0.17	0.55	−0.17	−0.58	−0.56	B4	3.77	0.15
4439	15.27	0.35	0.20	0.38	−0.03	−0.08	1.20	B9.5	3.82	0.15
1665	15.66	0.52	0.28	0.55	−0.05	−0.13	1.03	B9.5	3.82	0.16
4373	15.30	0.40	0.17	0.44	−0.06	−0.15	0.99	B9	3.88	0.16
5985	15.78	0.48	0.31	0.49	−0.03	−0.05	1.28	A0	3.92	0.16
4968	14.21	0.26	−0.16	0.39	−0.14	−0.45	0.01	B6	3.97	0.15
192	15.66	0.45	0.26	0.47	−0.04	−0.09	1.18	B9.5	4.01	0.16
4736	15.68	0.40	0.26	0.41	−0.02	−0.04	1.34	A0	4.10	0.16
1513	13.76	0.23	−0.29	0.39	−0.17	−0.57	−0.53	B4	4.14	0.16
2045	14.48	0.44	−0.11	0.60	−0.17	−0.55	−0.46	B4.5	4.15	0.17
4392	15.00	0.29	0.04	0.35	−0.07	−0.21	0.81	B8.5	4.18	0.16
3481	13.09	0.16	−0.44	0.36	−0.20	−0.70	−1.14	B3	4.19	0.16
716	14.78	0.23	−0.02	0.31	−0.08	−0.24	0.72	B8.5	4.19	0.16
4734	12.94	0.18	−0.47	0.39	−0.22	−0.76	−1.38	B2.5	4.22	0.16
2001	13.65	0.23	−0.32	0.40	−0.18	−0.61	−0.73	B4	4.23	0.17
5408	15.66	0.43	0.23	0.46	−0.04	−0.11	1.10	B9.5	4.24	0.17
3638	14.98	0.33	0.01	0.42	−0.09	−0.30	0.55	B8	4.25	0.17
4807	15.01	0.31	0.02	0.38	−0.08	−0.26	0.68	B8.5	4.26	0.17
1127	15.45	0.38	0.16	0.42	−0.05	−0.14	1.01	B9	4.26	0.19
1355	15.83	0.47	0.27	0.49	−0.04	−0.09	1.17	B9.5	4.26	0.17
3938	15.76	0.40	0.26	0.42	−0.02	−0.04	1.32	A0	4.27	0.17
798	13.98	0.21	−0.26	0.35	−0.16	−0.51	−0.29	B5	4.31	0.17
388	15.81	0.47	0.24	0.51	−0.05	−0.13	1.05	B9.5	4.36	0.18
1310	13.82	0.25	−0.30	0.42	−0.18	−0.61	−0.72	B4	4.43	0.17
5927	14.39	0.48	−0.16	0.66	−0.19	−0.65	−0.89	B3.5	4.45	0.18
1377	15.64	0.40	0.19	0.44	−0.05	−0.14	1.02	B9	4.46	0.18
1575	15.92	0.42	0.27	0.44	−0.03	−0.05	1.29	A0	4.52	0.18
1952	15.89	0.43	0.25	0.45	−0.03	−0.08	1.19	B9.5	4.57	0.19
4478	15.08	0.27	0.00	0.35	−0.08	−0.25	0.69	B8.5	4.59	0.18
2685	15.77	0.36	0.22	0.38	−0.03	−0.06	1.25	A0	4.64	0.18
2898	16.01	0.39	0.27	0.40	−0.01	−0.02	1.41	A0	4.73	0.19
514	15.18	0.28	0.01	0.35	−0.08	−0.25	0.71	B8.5	4.75	0.19
2776	15.47	0.34	0.10	0.39	−0.07	−0.19	0.87	B9	4.75	0.19
5564	15.73	0.39	0.17	0.43	−0.05	−0.15	1.00	B9	4.77	0.19
2010	15.09	0.21	−0.02	0.27	−0.07	−0.22	0.80	B8.5	4.89	0.20
1476	15.94	0.38	0.23	0.41	−0.03	−0.07	1.23	A0	4.91	0.20
5669	16.30	0.42	0.32	0.42	0.00	0.01	1.50	A0.5	4.99	0.20
1896	16.10	0.43	0.25	0.46	−0.04	−0.09	1.16	B9.5	5.04	0.20
4896	16.21	0.43	0.27	0.45	−0.03	−0.06	1.26	A0	5.16	0.22
4045	13.59	0.18	−0.44	0.38	−0.21	−0.72	−1.22	B3	5.30	0.21
3317	16.33	0.43	0.29	0.44	−0.02	−0.04	1.34	A0	5.31	0.22
356	16.03	0.37	0.19	0.41	−0.04	−0.11	1.10	B9.5	5.42	0.22
901	16.36	0.49	0.26	0.52	−0.05	−0.13	1.05	B9.5	5.45	0.22
4618	14.53	0.33	−0.25	0.50	−0.18	−0.62	−0.74	B4	5.53	0.22
217	15.47	0.39	−0.04	0.50	−0.13	−0.41	0.17	B6.5	5.62	0.23
1345	15.77	0.34	0.05	0.41	−0.08	−0.25	0.69	B8.5	5.79	0.23
2084	16.34	0.38	0.24	0.39	−0.02	−0.05	1.31	A0	5.82	0.24
1822	16.48	0.50	0.18	0.56	−0.08	−0.24	0.73	B8.5	6.33	0.26
383	16.78	0.44	0.29	0.46	−0.02	−0.05	1.31	A0	6.49	0.27
2975	16.21	0.39	0.05	0.47	−0.09	−0.29	0.58	B8	6.88	0.31
3592	16.90	0.42	0.29	0.43	−0.02	−0.03	1.38	A0	6.92	0.28
4959	17.09	0.46	0.32	0.46	−0.01	−0.02	1.39	A0	7.13	0.30
57	15.71	0.39	−0.11	0.52	−0.15	−0.49	−0.18	B5	7.16	0.29
5397	16.48	0.44	0.10	0.52	−0.09	−0.29	0.58	B8	7.16	0.29
5447	15.04	0.35	−0.26	0.53	−0.19	−0.65	−0.89	B3.5	7.22	0.29
2547	16.02	0.40	−0.04	0.52	−0.13	−0.42	0.11	B6	7.27	0.29
2899	16.77	0.39	0.20	0.42	−0.04	−0.11	1.11	B9.5	7.43	0.30
2491	16.37	0.42	0.04	0.51	−0.10	−0.34	0.42	B7.5	7.45	0.32

Table 4
(Continued)

ID	V	$B-V$	$U-B$	$E(B-V)$	$(B-V)_0$	$(U-B)_0$	M_V	Phot(ST)	Distance (kpc)	Δ Dist
4165	17.20	0.45	0.31	0.46	−0.02	−0.03	1.35	A0	7.61	0.32
3597	16.76	0.43	0.13	0.50	−0.08	−0.24	0.75	B8.5	7.86	0.33
920	17.21	0.50	0.26	0.53	−0.05	−0.13	1.04	B9.5	8.03	0.34
81	16.25	0.38	−0.04	0.49	−0.12	−0.40	0.20	B6.5	8.13	0.33
4503	17.13	0.42	0.24	0.45	−0.04	−0.09	1.17	B9.5	8.18	0.34
3025	14.67	0.30	−0.40	0.52	−0.22	−0.79	−1.51	B2.5	8.20	0.32
5113	16.76	0.38	0.11	0.44	−0.07	−0.21	0.82	B8.5	8.27	0.34
3275	17.24	0.44	0.26	0.47	−0.03	−0.08	1.21	B9.5	8.30	0.35
537	17.34	0.43	0.29	0.45	−0.02	−0.04	1.34	A0	8.37	0.35
188	14.24	0.16	−0.52	0.38	−0.22	−0.80	−1.56	B2.5	8.40	0.32
4263	16.77	0.39	0.10	0.45	−0.08	−0.24	0.75	B8.5	8.42	0.34
1209	16.17	0.29	−0.08	0.39	−0.11	−0.37	0.32	B7	8.49	0.34
5031	17.16	0.45	0.21	0.49	−0.05	−0.15	1.00	B9	8.52	0.35
68	16.79	0.42	0.07	0.50	−0.09	−0.30	0.56	B8	8.62	0.36
1205	17.11	0.41	0.19	0.46	−0.06	−0.15	0.99	B9	8.75	0.36
2765	17.19	0.43	0.19	0.48	−0.06	−0.16	0.96	B9	8.86	0.38
3736	17.09	0.46	0.14	0.53	−0.08	−0.25	0.70	B8.5	8.91	0.37
1903	16.06	0.25	−0.15	0.37	−0.13	−0.42	0.13	B6	9.09	0.36
411	15.53	0.25	−0.28	0.41	−0.17	−0.57	−0.54	B4	9.13	0.36
3750	14.12	0.21	−0.58	0.46	−0.25	−0.91	−2.21	B1.5	9.58	0.37
3299	16.28	0.39	−0.13	0.53	−0.16	−0.51	−0.29	B5	9.66	0.39
4327	17.68	0.44	0.28	0.46	−0.03	−0.06	1.26	A0	10.00	0.42
2866	15.61	0.31	−0.30	0.49	−0.19	−0.66	−0.93	B3.5	10.10	0.40
1289	17.36	0.38	0.16	0.42	−0.06	−0.15	0.99	B9	10.30	0.42
3958	17.84	0.46	0.30	0.47	−0.02	−0.05	1.29	A0	10.40	0.44
3174	17.67	0.46	0.22	0.49	−0.05	−0.14	1.02	B9	10.50	0.44
2071	16.85	0.39	−0.04	0.51	−0.13	−0.42	0.13	B6	10.70	0.44
744	17.71	0.45	0.23	0.48	−0.05	−0.12	1.07	B9.5	10.70	0.46
973	17.08	0.39	0.02	0.48	−0.10	−0.33	0.44	B7.5	10.80	0.44
2904	16.63	0.35	−0.12	0.48	−0.15	−0.47	−0.09	B5.5	11.10	0.45
3426	15.25	0.40	−0.40	0.64	−0.24	−0.88	−2.01	B1.5	11.30	0.46
3489	17.84	0.44	0.24	0.48	−0.04	−0.11	1.10	B9.5	11.30	0.48
1847	17.89	0.51	0.21	0.57	−0.07	−0.21	0.81	B8.5	11.60	0.49
4227	16.45	0.39	−0.18	0.55	−0.18	−0.59	−0.62	B4	11.80	0.48
1472	16.41	0.33	−0.21	0.49	−0.17	−0.56	−0.50	B4.5	12.00	0.48
1878	17.87	0.47	0.17	0.53	−0.07	−0.21	0.81	B8.5	12.20	0.52
3022	17.39	0.42	0.02	0.52	−0.11	−0.36	0.33	B7	12.30	0.51
2800	17.93	0.42	0.19	0.46	−0.06	−0.15	0.98	B9	12.70	0.54
3969	16.10	0.27	−0.32	0.46	−0.19	−0.66	−0.93	B3.5	13.30	0.52
5064	16.33	0.42	−0.26	0.61	−0.21	−0.72	−1.19	B3	13.30	0.54
2637	16.53	0.35	−0.23	0.52	−0.18	−0.61	−0.70	B4	13.40	0.54
1601	16.46	0.28	−0.25	0.44	−0.17	−0.57	−0.54	B4	13.50	0.53
3600	17.13	0.45	−0.10	0.60	−0.16	−0.53	−0.38	B4.5	13.60	0.56
857	18.12	0.40	0.20	0.44	−0.05	−0.13	1.06	B9.5	13.80	0.59
5052	17.24	0.42	−0.09	0.55	−0.15	−0.50	−0.22	B5	14.10	0.59
1740	17.91	0.32	0.13	0.36	−0.05	−0.13	1.04	B9.5	14.20	0.61
2833	18.02	0.44	0.11	0.51	−0.08	−0.26	0.66	B8.5	14.20	0.61
2956	17.82	0.41	0.04	0.50	−0.10	−0.33	0.46	B7.5	14.50	0.61
2498	16.83	0.48	−0.19	0.67	−0.20	−0.69	−1.07	B3	14.70	0.65
3331	17.63	0.40	−0.04	0.52	−0.13	−0.42	0.13	B6	15.10	0.63
4181	18.07	0.45	0.08	0.54	−0.10	−0.32	0.48	B7.5	15.20	0.65
528	18.49	0.47	0.23	0.51	−0.06	−0.15	0.99	B9	15.20	0.68
3059	18.05	0.43	0.07	0.51	−0.10	−0.31	0.51	B8	15.50	0.66
2986	18.46	0.44	0.21	0.48	−0.05	−0.14	1.00	B9	15.70	0.70
3826	17.66	0.38	−0.07	0.51	−0.14	−0.44	0.03	B6	16.30	0.68
6107	17.45	0.45	−0.11	0.60	−0.17	−0.56	−0.49	B4.5	16.40	1.46
3720	16.58	0.29	−0.32	0.48	−0.20	−0.67	−1.00	B3	16.50	0.66
1106	18.72	0.46	0.25	0.50	−0.04	−0.11	1.10	B9.5	16.50	0.76
955	18.77	0.48	0.26	0.51	−0.04	−0.11	1.10	B9.5	16.50	0.75
3763	16.80	0.45	−0.28	0.66	−0.22	−0.77	−1.43	B2.5	17.20	0.75
3641	17.25	0.32	−0.22	0.48	−0.17	−0.57	−0.54	B4	18.30	0.80
3148	16.45	0.29	−0.40	0.51	−0.22	−0.78	−1.46	B2.5	18.60	0.74
754	18.95	0.48	0.23	0.52	−0.06	−0.15	0.97	B9	18.80	0.91

Note. The last column indicates the error in distance.

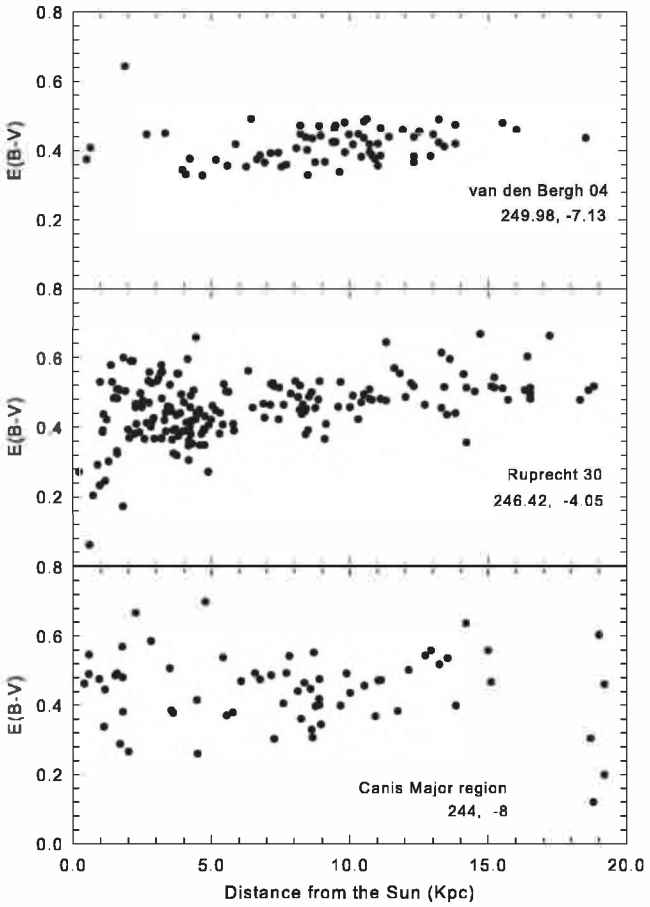

Figure 8. Trend of reddening as a function of heliocentric distance along the line of sight to VdB–Hagen 04 (upper panel) and Ruprecht 30 (middle panel). Lower panel shows the same trend for the CMa overdensity direction. Only stars earlier than A0 have been used. In the upper panel, the compact star cluster VdB–Hagen 04 is located at a distance of about 12 kpc.

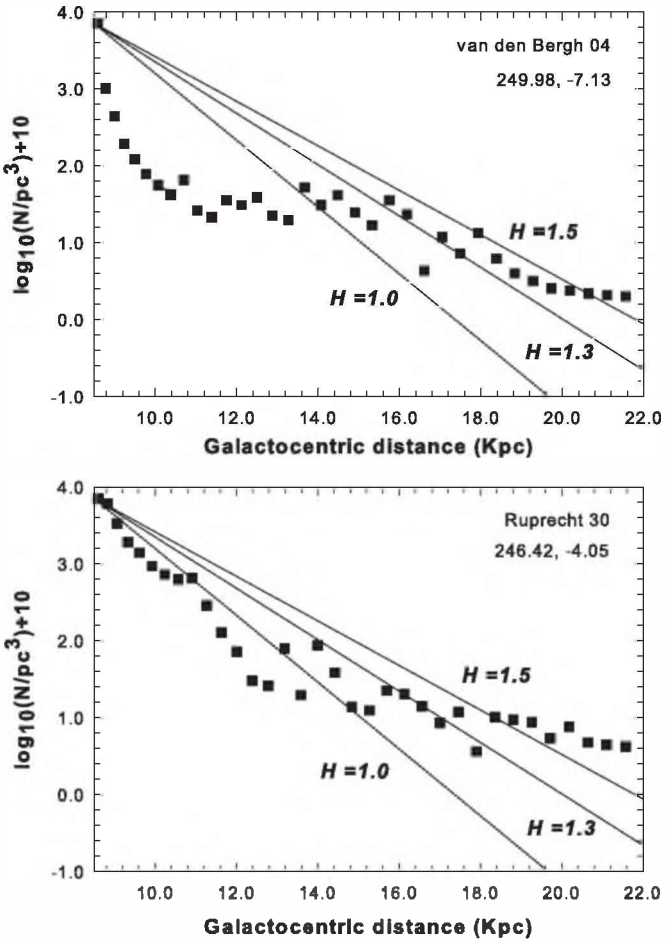

Figure 9. Density of stars in the direction of Ruprecht 30 (dashed symbols) and VdB–Hagen 04 (solid symbols). Density is expressed in star number per cubic parsec. Only stars earlier than A0 have been considered.

centered in the CMa overdensity ($l = 244°$, $b = -8°$), and derived by performing exactly the same analysis as above for the dataset presented in Carraro et al. (2008), properly normalized to take into account the same coverage area. Exactly as in the cases of VdB–Hagen 04 and Ruprecht 30, we find in this direction that the reddening jumps up immediately in the solar vicinity and stays almost constant all the way to the limit of our photometric dataset. No particular stars` lumps are evident; on the contrary, we find stars located almost uniformly from the Sun up to at least 15 kpc.

6. THE SPATIAL DISTRIBUTION OF YOUNG STARS IN THE OUTER DISK

The trend of young star density as a function of the heliocentric distance is shown in Figure 9. In this figure, star counts are expressed in stars per cubic parsec using half a kiloparsec as the distance bin. The dashed line refers to the field in the direction of Ruprecht 30, whereas the solid line corresponds to the field toward VdB–Hagen 04. The logarithmic counts are also shifted by an arbitrary value for the sake of visibility. In a few distance bins, we did not have any stars and had to interpolate linearly from neighboring bins.

The two distributions are similar up to 9 kpc from the Galactic center, they then fall down to about 13 kpc from the Galactic center. In this distance range, the star density goes down faster toward VdB–Hagen 04. This can be understood since VdB–Hagen 04 is at higher Galactic latitude than Ruprecht 30. At about 13 kpc from the Galactic center the two profiles cross and flatten up to 16 kpc, and then they keep falling down to ~22 kpc from the Galactic center, which corresponds to the limit of our photometry. The shape of the derived profile can be tentatively interpreted as follows. Along the two lines of sights and beyond half a kpc from the Sun the density drops until the Perseus arm is reached. We recall from previous studies of our group (Vázquez et al. 2008) that at the longitudes in consideration, the Local arm is not very important and therefore does not contribute many early-type stars beyond 500 pc from the Sun. The change of the slope between 13 and 16 kpc from the Galactic center probably indicates the presence and size of the Perseus arm in this region of the 3GQ, where the Galactic warp reaches its maximum height below the formal $b = 0°$ Galactic plane (Moitinho et al. 2006). Beyond 16 kpc from the Sun, we enter an almost empty region until the outer arm (Norma-Cygnus) is reached. This arm is quite extended and sparse, and—due to Galactic rotation—is very far away in this portion of the disk and does not contribute much in terms of young stars in the area that we are probing. Overall, however, the trend of star density in the outer disk looks more like an exponential trend with some structures than an abrupt cutoff as predicted by models.

To provide a more quantitative assessment, we fit the OBA star counts found in the direction of the regions of Ruprecht 30 and VdB–Hagen 04 by adopting a simple exponential law of the

form:

$$\rho(R, l, b, \text{age}) = \rho_0 \cdot e^{-(R-R_0)/H}, \quad (3)$$

where H (the scale length in kpc) is a free parameter. The same equation is valid for ages smaller than 100 Myr, typical for the OBA spectral-type stars we are considering here.

The galactocentric distance has been computed as

$$R = \sqrt{(R_0^2 + d^2 \times \cos b^2 - 2 \times R_0 \cdot d \cdot \cos l \cdot \cos b)} \quad (4)$$

and for R_0, the Sun distance to the Galaxy center, we adopted 8.5 kpc.

The normalization parameter of the local density for early-type stars, ρ_0, was taken from Reed (2001), where it was stated that the local density of OB-type stars is 9.12×10^{-7} stars pc^{-3}. This last value is somehow uncertain given the scarcity of stars of these spectral types in the solar neighborhood. Furthermore, let us mention that Robin & Crézé (1986a) report in their Table 2, values ranging from 0.6×10^{-7} to 0.5×10^{-4} for stars between O7 and A0 spectral types. At any rate, a rough estimate of the local density of OBA stars according to our own star counts yields a local density of 7.07×10^{-7} stars pc^{-3}, which is more in line with the Reed (2001) findings.

Three attempts were then made to fit star counts using scale lengths $H = 1.0$, $H = 1.3$, and $H = 1.5$ kpc. These values are adequately inserted between the range of scale lengths from 1.0 to 5.5 kpc for the thin disk, computed e.g., by Rong et al. (2001).

In all the three cases, the excess of OBA stars we found in our directions is evident and significant, and demonstrate that the Galactic thin disk extends much further than 14 kpc from the Galactic center. Besides, at large distances the thin disk appears as quite a disperse structure.

7. DISCUSSION AND CONCLUSIONS

We have provided evidence for the existence of young diffuse groups of B stars in the extreme periphery of the Galactic disk, at galactocentric distances between 14 and 22 kpc.

The two fields we have analyzed are centered on cataloged open clusters: VdB–Hagen 04 and Ruprecht 30. However, most of the young stars that we found are evenly distributed across the field and have quite a significant distance spread, both facts being incompatible with the presence of physical star clusters. We found only a marginal concentration in the center of Field 1, compatible with the small, distant star cluster VdB–Hagen 04 (Carraro & Costa 2007).

The results presented here, together with those from other groups (Snell et al. 2002; Yun et al. 2007, 2009; Brand & Wouterloot 2007), demonstrate that the Galactic thin disk does not have a sharp cutoff at $R \sim 14$ kpc, contrary to what has been commonly believed, and that active star-forming regions are present in its outer limits. Our results also show that, as indicated by the values of Z_{GC} given in Table 1, the thin disk bends considerably in the 3GQ, emphasizing once more the importance of the Galactic warp (Momany et al. 2004, 2006; Moitinho et al. 2006).

We recall that the overdensity of stars we found in the outer disk beyond the model cutoff is not limited to OAB stars (thin disk), but extends to M giant stars—in the thick disk—as well, as recently shown by Momany et al. (2006).

Our findings indicate that a major revision of the Galactic models that aim to predict the stellar population in the outer Galactic disk is required.

The authors express their gratitude to the referee for a number of valuable suggestions, which helped to improve the quality of the paper. G.C. is grateful to K. Janes, Y. Momany, T. Bania, and D. Russeil for their useful input. This study made use of Simbad and WEBDA databases. E.C. acknowledges support by the Chilean Centro de Astrofísica (FONDAP No. 15010003) and the Chilean Centro de Excelencia en Astrofísica y Tecnologías Afines (PFB 06).

REFERENCES

Brand, J., & Wouterloot, J. G. A. 2007, A&A, 464, 909
Carraro, G., & Costa, E. 2007, A&A, 464, 573
Carraro, G., & Costa, E. 2009, A&A, 493, 71
Carraro, G., Moitinho, A., & Vázquez, R. A. 2008, MNRAS, 385, 1597
Carraro, G., Moitinho, A., Zoccali, M., Vázquez, R. A., & Baume, G. 2007, AJ, 133, 1058
Carraro, G., Vázquez, R. A., Moitinho, A., & Baume, G. 2005, ApJ, 630, L153
Dias, W. S., Alessi, B. S., Moitinho, A., & Lépine, J. R. D. 2002, A&A, 389, 871
Fitzgerald, M. P. 1968, AJ, 73, 983
Janes, K. A. 1991, in Precision Photometry: Astrophysics of the Galaxy, ed. A. G. D. Philip, A. R. Upgren, & K. A. Janes (Schenectady, NY: Davis Press), 233
Landolt, A. 1992, AJ, 104, 340
Martin, N. F., Ibata, R. A., Bellazzini, M., Irwin, M. J., Lewis, M. J., & Dehnen, W. 2004, MNRAS, 348, 12
Moffat, A. F. J., Jackson, P. D., & Fitzgerald, M. P. 1979, A&AS, 38, 197
Moitinho, A. 2001, A&A, 370, 436
Moitinho, A., Vázquez, R. A., Carraro, G., Baume, G., Giorgi, E. E., & Lyra, W. 2006, MNRAS, 368, L77
Momany, Y., Zaggia, S., Bonifacio, P., Piotto, G., de Angeli, F., Bedin, L. R., & Carraro, G. 2004, A&A, 421, L29
Momany, Y., Zaggia, S., Gilmore, G., Piotto, G., Carraro, G., Bedin, L. R., & de Angeli, F. 2006, A&A, 451, 515
Newberg, H. J., et al. 2002, ApJ, 569, 245
Patat, F., & Carraro, G. 2001, MNRAS, 325, 1591
Reed, B. C. 2001, PASP, 113, 537
Robin, A. C., & Crézé, M. 1986a, A&A, 157, 71
Robin, A. C., & Crézé, M. 1986b, A&AS, 64, 53
Robin, A. C., Crézé, M., & Mohan, V. 1992, ApJ, 400, L25
Rong, J., Buser, R., & Karaali, S. 2001, A&A, 365, 431
Ruprecht, J. 1966, Bull. Astron. Inst. Czechoslovakia, 17, 33
Sale, S. E., et al. 2010, MNRAS, 402, 713
Schmidt-Kaler, T. 1982, Landolt-Bornstein, Group VI, Vol. 2b, Stars and Star Clusters (Berlin: Springer), 15
Skrutskie, M. F., et al. 2006, AJ, 131, 1163
Snell, R. L., Carpenter, J. M., & Heyer, M. H. 2002, ApJ, 578, 229
Stetson, P. B. 1987, PASP, 99, 191
Straizys, V. 1995, Multicolor Stellar Photometry: Astronomy and Astrophysics Series (vol. 15; Tucson, AZ: Pachart)
van den Bergh, S., & Hagen, G. L. 1975, AJ, 80, 11
Vázquez, R. A., Baume, G., Feinstein, C., Nunez, J. A., & Verge, N. M. 2005, A&A, 430, 471
Vázquez, R. A., May, J., Carraro, G., Bronfman, L., Moitinho, A., & Baume, G. 2008, ApJ, 672, 930
Vázquez, R. A., Moitinho, A., Carraro, G., & Dias, W. 2010, A&A, 511, 38
Yun, J. L., Elia, D., Palmeirim, P. M., Gomes, J. L., & Martins, A. M. 2009, A&A, 500, 833
Yun, J. L., López-Sepulcre, A., & Torrelles, J. M. 2007, A&A, 471, 573